NASA Contractor Report 159266

(NASA-CR-159266) DIGITAL SIMULATION OF DYNAMIC PROCESSES IN RADIOMETER SYSTEMS Contractor Report, 1 Jan. - 31 Dec. 1978 (Old Dominion Univ. Research Foundation) 48 p HC A03/MF A01 CSCL 09C G3/33

N80-23563

Unclas 20142

DIGITAL SIMULATION OF DYNAMIC PROCESSES IN RADIOMETER SYSTEMS

William D. Stanley

OLD DOMINION UNIVERSITY RESEARCH FOUNDATION
Norfolk, Virginia 23508

NASA Contract NAS1-14193, Task 46
May 1980

National Aeronautics and Space Administration

Langley Research Center
Hampton, Virginia 23665

DEPARTMENT OF ELECTRICAL ENGINEERING
SCHOOL OF ENGINEERING
OLD DOMINION UNIVERSITY
NORFOLK, VIRGINIA

DIGITAL SIMULATION OF DYNAMIC PROCESSES IN RADIOMETER SYSTEMS

By

William D. Stanley
Principal Investigator

Final Report
For the period January 1 - December 31, 1978

Prepared for the
National Aeronautics and Space Administration
Langley Research Center
Hampton, Virginia 23665

Under
Master Contract Agreement NAS1-14193
Task Authorization No. 46
William F. Croswell, Technical Monitor
Flight Electronics Division

Submitted by the
Old Dominion University Research Foundation
P. O. Box 6369
Norfolk, Virginia 23508

TABLE OF CONTENTS

LIST OF FIGURES

TECHNIQUES FOR DIGITAL RADIOMETER DESIGN

By

William D. Stanley[1]

INTRODUCTION

This report describes the development, format, and statistical verification of a number of computer programs which simulate various classes of microwave radiometers. These programs should provide valuable assistance in developing new systems and in evaluating the performance of existing systems. All of the programs are dynamic in nature, and most employ random signals in the simulation. In this manner, the actual random processes encountered in radiometers are closely represented, and the resulting responses can be made to correspond closely with "real-life" situations in a statistical sense.

In addition to this report, two other publications have resulted from the present grant: a conference paper which has been presented and a journal paper which has been accepted for publication. Bibliographical data for these publications are given at the end of the "References" section. Another report based on work initiated under this grant but continued under a separate contract is expected to be completed in the near future.

Since the present report is primarily concerned with the development and verification of simulation models, only those details of radiometer performance relevant to that objective are discussed. Results are drawn freely from the literature as needed. The future report mentioned in the preceding paragraph will deal specifically with the detailed derivation of many of the performance characteristics not widely available elsewhere, and some of these results are included in the present report when required.

All of the programs developed are available to appropriate engineering personnel at NASA/Langley Research Center (LaRC) through the cooperative

---

[1] Professor and Graduate Program Director, Department of Electrical Engineering, Old Dominion University, Norfolk, Virginia 23508.

activities between that organization and Old Dominion University (ODU). However because of recent policies of the For Early Domestic Dissemi ation (FEDD) program and the unwieldy nature of the actual programs, detailed instructions are not provided in this report. Thus, the major emphasis in the report is devoted to the general approach used in developing the programs, a discussion of the major problems that had to be circumented, the means by which the problems were resolved, and a general verification of the validity of the simulations.

GENERAL APPROACH

As a starting point for this development, consider the simplified total power radiometer block diagram shown in figure 1. The function representing the desired signal whose statistical variance is to be measured is $X_A(t)$, which is a random process with an effective noise temperature T_A. Added to this signal is the noise $X_R(t)$ generated by the receiver, which has an effective noise temperature T_R.

Following some possible amplification, the signal is filtered by a wide-band input filter which limits the bandwidth to the range over which the effective temperature is to be measured. This filtered noise is then detected by a square-law detector, and the mean value of the output is proportional to the noise temperature at the input. A narrow-band output filter then smoothes the signal and provides an output signal $V(t)$.

The output signal $V(t)$ of the low-pass filter is a statistical estimate of the total system input temperature. The mean value $\overline{V}$ contains the desired measurement (as well as a bias component), but there are two significant factors that contribute to fluctuations in the output: (1) Since both $X_A(t)$ and $X_R(t)$ are random processes, there will always be fluctuations due to the noiselike nature of these processes. Such effects will be referred to as "noise fluctuations," and the standard deviation of $V(t)$ due to these fluctuations will be denoted as "σ_{vn}." (2) Small variations in the gains of the various amplifier stages are usually present, and they contribute to fluctuations in the output. The standard deviation of $V(t)$ due to these variations will be denoted as "σ_{vg}."

A computer simulation model for a microwave radiometer must meet a number of specific requirements: (1) The program must contain a number of statistically independent, random Gaussian noise sources, each with precisely controllable mean and variance. (2) The program should have the capability of simulating transfer functions of reasonably high order to properly represent the effects of both predetection and postdetection filtering. (3) Precision numerical integration routines should be available for simulating the continuous-time operations involved. (4) As digital processing methods are investigated, the program should be directly adaptable for discrete-time operation. (5) On the Dicke radiometer, modulation operations at both the input and output are

required. (6) Means should be available for verifying the validity of the simulations to a high degree of statistical accuracy.

While it is possible to develop programs "from scratch" that will achieve the required goals, a more sensible approach seemed to be the use of one of the standard system simulation programs. Specifically, the modeling process was initiated with the Continuous System Modeling Program (CSMP, System 360). This program was developed by IBM and was readily available in the software library of the DEC-10 system at ODU.

CSMP is a system-oriented program that allows direct simulation of a system from either the various block diagrams or from the system differential equations. Both linear and nonlinear components may be simulated, and both time-varying and time-invariant systems may be represented. The numerous properties of CSMP are discussed in detail in references 1, 2, and 3 and will not be discussed here except as they relate to the simulation of radiometers. Use of the system blocks is made freely in the developments that follow.

After the development work on the simulation models was well under way, it appeared desirable to transfer the various programs to NASA/LaRC so that they could be available to personnel there and because only limited finances were available in the contract for continued development at ODU. After some investigation, it appeared that a comparable version of CSMP was not readily available at NASA/LaRC; however, the Advanced Continuous Simulation Language (ACSL) (ref. 4) was readily available, so the work was converted to that language. Although there are minor programming differences in some of the details, both languages have displayed approximately equal capabilities as far as radiometer simulation is concerned.

As simulation details were developed, it was noted that two boundary conditions on the simulation capability were the widest bandwidth in the system (momentarily denoted as B) and the simulated time (momentarily denoted as T) of the measurement. The number of total computations is proportional to the product BT, and the computational time increases approximately linearly with BT after some time is allowed for initialization and sorting.

In actual radiometer systems, B varies from perhaps 10 MHz to 2 GHz or more, while T varies from perhaps 100 ms to 10 s or more. Consequently,

BT might vary from 10^6 to greater than 2×10^{10}. It was found that actual simulation runs with realistic BT products could cost several hundred dollars per run. While such a run might be economically feasible in investigating a new design or concept, it is not usually feasible for routine simulation checks or, as in the case at hand, in the development of the simulation programs themselves, which necessitates many routine runs and checks.

The problem was alleviated by normalizing the BT products used to much smaller values for simulation purposes. It can be shown that the fluctuation of the output estimate is proportional to $1/\sqrt{BT}$. This means that the fluctuations are much greater than those of the real systems being simulated. However, provided that a proper mechanism for statistical verification is used, and provided that the user expects to deal with larger fluctuations than would be present in the real system, this effect can be tolerated.

TOTAL POWER RADIOMETER MODELS

The earliest and simplest form of a radiometer measurement system is the total power radiometer. While the total power radiometer has been largely superseded by more sophisticated systems for most current applications, a considerable portion of time was spent in developing and refining simulation models for this basic system, and a large portion of this report deals with this phase of the development. Operation and performance of the total power radiometer are understood much better than those of other systems, and the validity of the simulation programs can be more readily verified. In addition, the various functions developed for the total power radiometer can be readily incorporated in the more elaborate systems. Thus, most of the detailed discussions concerning total power component operation provided in this section are directly applicable to other classes of radiometers.

Consider again the block diagram of the total power simulation model shown in figure 1. The antenna input signal $X_A(t)$ is a Gaussian random variable having zero mean and a variance σ_A, whose normalized form will be discussed shortly. The noise contributed by the receiver $X_R(t)$ is also a Gaussian variable with zero mean, and it has a variance σ_R. These functions are generated by the Gaussian random number generator routines available in both CSMP and ACSL. It is absolutely necessary that these noise sources (as well as others that arise later) be statistically independent of each other, and this can be achieved by starting the processes with different "seed" numbers for the number-generator algorithms.

The available noise power from the antenna in an actual radiometer is KT_AB, and the noise from the receiver referred to the input is KT_RB, where T_A and T_R are the antenna and receiver effective noise temperatures referred to the input, K = Boltzmann's constant = 1.38×10^{-23} joules/kelvin, and B is the equivalent noise bandwidth. For typical values of T_A, T_R, and B, the actual power level is quite small at the input. However, large gains for predetector and postdetector amplifier stages result in a final output signal that might be of the order of several volts.

From a simulation point of view, it was decided early in the development to employ a normalized level for the signals so that the output values could be read directly in temperature for the total power models. This process was

continued for the Dicke models as well. However, when the closed-loop models were developed, it was found more desirable to return to absolute level simulation. Either approach is valid provided that all the gains and gain fluctuations have been appropriately normalized and adjusted.

A basic question that must be raised at the outset is that of defining the equivalent noise bandwidth for the noise generators at the input. In effect, the noise generator is "white," but since the signal is now a sampled signal, the bandwidth is not infinite, but instead is one-half the sampling frequency. Thus, "white noise" in a sampled system is noise defined over the bandwidth representing the highest unambiguous frequency. Actually, one could define a "two-sided" bandwidth which would be the sampling frequency itself, but it seemed more logical to remain within the context of a one-sided bandwidth since all subsequent system bandwidths are defined the same way.

The bandwidth B_p over which the noise power levels of the noise generators are defined is then given by

$$B_p = \frac{f_s}{2} = \frac{1}{2\Delta T} \tag{1}$$

where f_s = sampling frequency of the process and $\Delta T = 1/f_s$ = time between successive samples. (The frequency B_p is referred to in a sampling context as the "folding frequency.") Because the noise power is divided over a bandwidth which is a function of the sampling rate, it is absolutely essential that fixed interval sampling be employed in the simulation of such random processes. This precludes the possibility of using any of the variable step integration methods in the simulation of random process phenomena.

Having established the bandwidth over which the input noise is defined, the noise spectral density may then be computed. Assuming a flat noise spectrum over the bandwidth, the antenna noise spectral density function $G_A(f)$ and the receiver noise spectral density function $G_R(f)$ may be determined as follows:

$$G_A(f) = KT_A = \frac{P_A}{B_p} = \frac{2P_A}{f_s} = 2\Delta T P_A \tag{2}$$

$$G_R(f) = KT_R = \frac{P_R}{B_p} = \frac{2P_R}{f_s} = 2\Delta T P_R \tag{3}$$

where P_A and P_R represent the total required antenna power and receiver power, respectively. It is interesting to observe that P_A and P_R are specified directly to the noise generators and these values are independent of the sampling rate. However, the manner in which the power distributes itself over the bandwidth is a function of the sampling rate. Thus, for a given specified power, the noise spectral density is inversely proportional to the sampling rate.

Assume that the equivalent noise bandwidth of the input wide-band filter (to be discussed later) is B_{ni}. In order for the output estimate to be a direct reading of temperature, it is necessary to define a "normalized form of Boltzmann's constant" in the various power expressions. This quantity is denoted as K_n and is computed as

$$K_n = \frac{1}{B_{ni}} \tag{4}$$

From equations (2) and (3) with K_n replacing K, the quantities P_A and P_R are determined to be

$$P_A = \sigma_A^2 = K_n T_A B_p \tag{5}$$

$$P_R = \sigma_R^2 = K_n T_R B_p \tag{6}$$

where it is recognized that $P_A = \sigma_A^2$ is the variance of Gaussian process A, and $P_R = \sigma_R^2$ is the variance of Gaussian process R.

In calling the Gaussian functions in either CSMP or ACSL, $\sigma_A = \sqrt{P_A}$ = RMS value (or standard deviation) of source A and $\sigma_R = \sqrt{P_R}$ = RMS value of source R are the quantities that are employed in the arguments of the Gaussian number generators. It will be shown shortly that this seemingly odd choice of K_n will produce the desired normalized output.

The input wide-band filter is discussed next. This filter represents in an actual radiometer the bandwidth over which the total noise power measurement is made. As the bandwidth is increased, both the number of equivalent statistically independent samples per unit time appearing at the detector input and the total detector input power increase. The variance of the output estimate

decreases as a result, but the frequency resolution of the estimate decreases. Thus, there is a direct tradeoff between the variance of the output estimate and the frequency resolution over which the measurement is desired. The only way in which both may be increased is by means of a longer integration time. Typical values of input bandwidth range from 10 MHz or less to 2 GHz or more. As previously noted, it is very difficult to simulate actual bandwidths without consuming excessive computer time, and so some frequency scaling is normally required.

At the beginning of the simulation effort, a decision was made to employ a 10-pole Butterworth filter as the input wide-band filter with the 3-dB bandwidth BCIN selectable as a program input. The reasons for this filter choice were as follows: (1) The Butterworth function is a good "middle of the road" characteristic which is representative of filter types employed in many radiometer receivers. Although not quite as sharp as the Chebyshev and elliptic function types, it is simpler in form and easier to manage both mathematically and in simulation form than the other types mentioned. (2) The choice of 10 poles provides a slope of -60 dB/octave or -200 dB/decade in the stopband, and the result is a good approximation to an ideal block characteristic. This provides some safeguard on possible aliasing errors that might have to be considered if the sampling rate were not much higher than twice the actual filter bandwidth.

As a result of this choice, a number of simulation results was developed around the 10-pole Butterworth filter, and much of the data tabulated later in the report were obtained from that form. However, some difficulties were encountered in the Dicke model for reasons that will be discussed in the next section. These were difficulties that would be readily circumvented if enough computer time were available, but due to computer time limitations, it was decided to investigate the use of a lower order filter.

For studies made with a lower order filter, the three-pole Butterworth was selected. This filter provides an 18 dB/octave or a 60 dB/decade rolloff rate, which is significantly less than that of the 10-pole filter but is manageable provided that several precautions are observed: (1) More attention should be paid to possible aliasing errors; hence it may be necessary to ensure that the sampling rate be well above the minimum possible value for most applications.

(2) The equivalent noise bandwidth is nearly 5 percent greater than the 3-dB bandwidth; specifically $B_{ni} = 1.047 \times$ (3-dB bandwidth), and this fact must be noted in the fluctuation analysis.

The realizations of both filters were achieved through the use of CSMP and ACSL system macros. Both languages provide separate one-pole and two-pole transfer function blocks. The 10-pole Butterworth filter was implemented with 5 2-pole sections, and the 3-pole Butterworth filter was implemented with 1 2-pole section and 1 1-pole section.

Following the filter is the square-law detector, which produces an output voltage proportional to the square of the input voltage. This is equivalent to the fact that the output voltage is directly proportional to the input power. Not all radiometer detectors are square-law detectors, but they are by far the most common and have been determined to be as good as any other form.

It can be shown that when the input voltage to a square-law device has a Gaussian distribution, the output has a chi-square distribution with one degree of freedom. In the frequency domain, the flat power spectrum at the input is converted to a triangular power spectrum plus an inpulse at dc. The impulse represents the square of the mean-value of the detector output voltage which results from the squaring operation of the detector, and the triangular spectrum represents the unfiltered fluctuations of the output estimate. The signal is then applied to a very narrow band low-pass filter, which passes the inpulse without alteration, but in which the variance of the estimate is reduced drastically.

Assuming a reference normalized gain level of unity throughout the system, the expected value $\overline{V}$ of the output estimate is

$$\overline{V} = \left(\frac{P_A + P_R}{B_p}\right) B_{ni} = K_n (T_A + T_R) B_{ni} \tag{7}$$

The definition of K_n given by equation (4) yields an expected value $\overline{V}$ of the normalized output estimate of

$$\overline{V} = T_A + T_R \tag{8}$$

Thus, the desired goal of having a direct reading of temperature for the expected value of the output is achieved.

Some discussion of the postdetector output filter is required. Many references use the "running integrator" filter as the basis for analysis of the measurement process. Ideally this circuit integrates the signal for an interval T, divides by the interval time, and provides an output $V(T)$ given by

$$V(T) = \frac{1}{T}\int_0^T V_i(t)\, dt \tag{9}$$

where $V_i(t)$ is the input signal. The steady-state transfer function $H(f)$ of this filter can be shown to be

$$H(f) = \frac{\sin \pi fT}{\pi fT} \tag{10}$$

and the dc gain is simply $H(o) = 1$. The equivalent noise bandwidth B_{no} for the running integrator is

$$B_{no} = \frac{0.5}{T} \tag{11}$$

There are several advantages of the running integrator as an estimator for the mean value of the process: (1) The actual time of integration T is exactly the same as the specified "integration time," with the latter term being a widely employed but potentially ambiguous and misleading term for other filter types. (2) The settling time of the filter is short compared to many (but not necessarily all) common filters, resulting in a relatively short time in obtaining an estimate. (3) The ratio of the variance of the output estimate to the mean value decreases as $1/\sqrt{T}$, meaning that the accuracy of the estimate continues

to improve with integration time. With a large number of filters, the variance is reduced during the settling time, but a point is reached in which no further reduction occurs as time continued to increase.

In spite of these advantages, the running integrator suffers from one disadvantage when applied to a Dicke switching radiometer. The problem concerns the fact that harmonics at multiples of the switching frequency are not attenuated very well and may appear in significant size at the output. This problem will be discussed at greater length in the next section and is, of course, not relevant to the total power radiometer.

A second and less significant disadvantage is that a running integrator requires an active realization, which results in the possibility of stability and offset difficulties, while many other filter types can be achieved with simple passive networks.

Two final points concerning the total power simulation shown in figure 1 deserve mention. Random gain fluctuations may be produced by the block with the parameter AVDEL. This quantity represents the standard deviation of a random variable representing a per unit voltage gain fluctuation to the right of the square-law detector. Through the squaring relationship of the detector, a gain fluctuation on either side may be represented at this point provided that the appropriate level is used. Since rapid variations in gain fluctuations are partially suppressed by the output filter, the strategy used is to select a worst-case condition of a fixed change in gain which remains at the new value until changed by the program.

The final parameter to be discussed in KFVG, which represents a "forward voltage gain constant." This parameter can be used to establish any arbitrarily desired level for the overall gain. In many of the simulation runs using the normalizing process discussed earlier, KFVG was set to unity.

DICKE SWITCHING RADIOMETER MODELS

A block diagram of the basic Dicke switching radiometer model is shown in figure 2. This particular model utilizes the widely employed square-wave correlation principle. Although a few systems employ sine-wave correlation and it is felt that the square-wave model could be readily adapted to such a strategy, only square-wave correlated systems have been simulated thus far.

In the Dicke system, the input to the wide-band predetection filter is alternately switched between the input antenna signal $X_A(t)$ and a reference signal $X_B(t)$ whose effective noise temperature T_B is known to a high degree of accuracy. The receiver noise $X_R(t)$ appears as sort of a "common-mode" signal and is added to the noise at the Dicke switch on both halves of the switching cycle. The signal is then filtered by a wide-band predetection filter and processed by a square-law detector.

At the output of the square-law detector, a second synchronous Dicke switch alternately switches the signal between paths having gains of +1 and -1. The inversion causes a cancellation of the mean value of the receiver temperature. The result is that the mean value $\overline{V}$ of the output estimate is not a function of the receiver temperature, thus eliminating a significant source of uncertainty present in the total power radiometer. However, since the actual signal $X_A(t)$ is only observed for half of the total time in the Dicke radiometer, a subsequent loss in sensitivity results. In addition, gain fluctuations are not completely eliminated by the Dicke process, although they are generally reduced in intensity.

In the case of the open-loop Dicke simulations, the normalized form of Boltzmann's constant was chosen to be

$$K_n = \frac{2}{B_{ni}} \tag{12}$$

The factor of two was used because of the fact that the Dicke switching operation introduces a factor of one-half in the effective gain of the mean of the process. The result is that the mean value of the output turns out to be simply

$$\overline{V} = T_A - T_B \tag{13}$$

so that a direct reading of temperature can be obtained.

Some difficulty was encountered with the 10-pole Butterworth filter with Dicke systems. The problem arose because of the BT reduction necessary for the simulation as has already been discussed. A 10-pole Butterworth filter has a rather long settling time and a significant amount of delay time, both of which are on the order of several times the reciprocal of the bandwidth. To provide appropriate output correlation with the Dicke switch, it is necessary that the delay be insignificant compared with the time duration of half a cycle of the Dicke frequency. The error arising from the delay and settling time with the 10-pole Butterworth was judged to be too severe for the BT products employed. Subsequently, a three-pole Butterworth filter was found to be adequate provided that allowance for the additional bandwidth was made in noise power computations and provided that the BT product was increased to about 100 times the Dicke switching frequency.

Another problem that arose in the Dicke simulation was that of ripple in the output. Because of the switching nature of the input to the receiver, Fourier components appear in the output at the switching frequency and its harmonics. This disturbance represents a deterministic fluctuation which adds to the noise fluctuations which are random in form. An analysis was made to predict the level of the ripple, and measurements verified the level predicted. Since this phenomenon is also a problem in real Dicke radiometers, any means employed to reduce its intensity can be adapted to an actual radiometer system.

FEEDBACK RADIOMETER MODELS

The largest single effort in this study has been the analysis and development of a series of models for closed-loop, noise-injection radiometers. In fact, because of the formidable nature of this chore, the lack of good supporting analytical efforts, and the fact that this development is still continuing under a different contract, only a minimal amount of actual simulation data concerning these models is presented in this report. However, it should be strongly emphasized at the outset that successful programs have indeed been developed, and the partial redesign of an existing tracking loop has already been achieved as a result of a feedback simulation study. Simulation runs of a closed-loop model are relatively expensive, and since there is a degree of uncertainty in the theoretical analysis needed to fully support these simulation results, the data obtained does not lend itself to the same degree of verification utilized in the open-loop models.

Two particular forms of models have been developed for the feedback systems. The first class is comparable to the types already discussed for open-loop systems and will be denoted as a "statistical" form. The statistical form employs random processes throughout and is used to study the statistical estimation process.

The second class will be denoted as a "deterministic" form and is used to study the actual control mechanism of the loop and its relative stability (or instability). In this form, the random processes are replaced by their equivalent temperature values on a power basis, and the basic dynamic behavior of the loop is exhibited without the additional complication of the noise processes being present. Both forms have been found useful in the modeling of closed-loop systems.

The basic form of the statistical closed-loop radiometer model is shown in figure 3. The signal $X_A(t)$ represents the input signal from the antenna whose effective brightness temperature T_A is to be determined. In a typical closed-loop radiometer, the feedback sygnal is added to the input signal in a directional coupler. The constant 1-KDIRCP represents the fractional power of the input signal contributing to the forward output power and is typically 0.99. The injected noise signal is added through the auxiliary arm and has a power gain constant KDIRCP, which is typically 0.01 (-20 dB).

The actual injected noise typically consists of noise pulses from a controlled noise generator, such as a hot carrier diode, plus the ambient noise related to temperature of the enclosure. The noise pulses are turned on by the output signal of the loop and serve as the feedback mechanism to maintain closed-loop operating conditions. The noise signal produced by the noise diode is denoted by $X_D(t)$, and this function can be characterized by an effective noise temperature T_D, representing the actual noise temperature of the diode. However, it may also be characterized by an "excess" noise temperature TEXCNS, which is the temperature by which the noise diode exceeds the controlled temperature T_B of the enclosure, i.e. TEXCNS = $T_D - T_B$. The concept of the excess noise was utilized in most of the simulation programs developed and was found to be the most convenient form.

The enclosure is maintained at a constant temperature T_B, whose value is known to a high degree of accuracy. The noise signal $X_B(t)$ corresponding to T_B is added to the excess noise from the diode source, and the result is applied to the directional coupler.

From the output of the directional coupler, the signal is processed with a Dicke radiometer in the same fashion as for an open-loop radiometer. However, the output of the postdetection filter is connected back to the noise-injection block in order that a sufficient amount of feedback noise can be injected to maintain a closed-loop condition. Under ideal steady-state conditions, the sum of T_A plus the feedback noise temperature is exactly equal to T_B, and the effect of gain fluctuations is eliminated. In other words, the output estimate is a function only of feedback parameters and not of forward gain parameters, so that steady-state fluctuations in forward gain parameters do not contribute to error. (During transient or changing input temperature conditions, gain fluctuations may contribute to errors in the estimate.)

The form of the deterministic model is shown in figure 4. The various quantities on the block diagram are generally related to those in figure 3 except that no statistical parameters are used. Instead, the mean values of the processes are represented on a power basis. This means that some of the quantities involved are the squares of the corresponding parameters in figure 3, which was shown primarily in terms of linear (or voltage) quantities where appropriate.

A few terms that have not been previously discussed will now be defined. The quantity KFVG represents a forward voltage gain constant for the statistical model, and KFPG represents the corresponding forward power gain constant for the deterministic model. The quantity KVTENR represents the voltage to excess noise ratio constant appearing in the feedback loop. The quantity KINT represents the integrator constant, and the loop filter represents any additional transfer function used to establish the proper dynamic loop response and data smoothing. Several different forms of loop filters have been simulated thus far. Finally, it should be noted that several parameters are specified directly as power terms, which means that the square roots of these quantities are used on the block diagram in figure 3 (but not in figure 4).

STATISTICAL PARAMETERS AND SENSITIVITY

In this section, a summary of the various expressions for determining the mean-square fluctuations and sensitivity functions for several different types of radiometers is given. These relationships were used in the statistical verification of many of the simulations as is shown in the next section of the report.

The results employed are presented here without any proof or discussion of their origin. A separate report is currently being prepared which will deal specifically with the detailed development of these and other similar relationships. Certain of these relationships may be found in various parts of the literature, but it suffices to say at this point that the developments are so unwieldy that it would distract from the specific objectives of this report to present more than a brief summary.

First, consider the total power radiometer. The square of the mean value of the output estimate is given by

$$(\overline{V})^2 = C^2\left[\int_0^\infty |H_i(f)|^2\,df\right] H_o^2(0)\,(T_A + T_R)^2 \tag{14}$$

where $H_i(f)$ is the transfer function of the predetection filter, $H_o(f)$ is the transfer function of the output filter and C is a constant for the radiometer. The variance of the estimate σ_{vn}^2 due only to the noise fluctuations is given by

$$\sigma_{vn}^2 = 2C^2\left[\int_0^\infty |H_i(f)|^4\,df\right]\left[\int_0^\infty |H_o(f)|^2\,df\right](T_A + T_R)^2 \tag{15}$$

The ratio of σ_{vn}^2 to $(\overline{V})^2$ is

$$\frac{\sigma_{vn}^2}{(\overline{V})^2} = \frac{2\left[\int_0^\infty |H_i(f)|^4 \, df\right]\left[\int_0^\infty |H_o(f)|^2 \, df\right]}{\left[\int_0^\infty |H_i(f)|^2 \, df\right]^2 H_o^2(0)} \tag{16}$$

The standard definition of the equivalent noise bandwidth B_{no} as applied to the output filter is

$$B_{no} = \frac{1}{H_o^2(0)} \int_0^\infty |H_o^2(f)|^2 \, df \tag{17}$$

A definition peculiar to measurements made with square-law devices is a quantity referred to by Bendat and Piersol (ref. 5) as the "equivalent statistical bandwidth," by Tiuri (ref. 6) as the "RF bandwidth," and by Evans and McLeish (ref. 7) as the "reception bandwidth." The term "equivalent statistical bandwidth" is used in this report and is denoted as B_{si} as applied to the input filter. For this filter, B_{si} is defined as

$$B_{si} = \frac{\left[\int_0^\infty |H_i(f)|^2 \, df\right]^2}{\int_0^\infty |H_i(f)|^4 \, df} \tag{18}$$

By applying the definitions of equations (17) and (18) to equation (16) and taking the square root of both sides, the following rather simple result in obtained for the total power radiometer:

$$\frac{\sigma_{vn}}{\overline{V}} = \sqrt{\frac{2B_{no}}{B_{si}}} \tag{19}$$

Assume now that gain fluctuations are present and denote the RMS voltage gain fluctuation referred to a point after the square-law detector as ΔA. If the mean value of this gain is denoted as A, the per unit RMS fluctuation σ_{vg} of the output estimate is simply

$$\frac{\sigma_{vg}}{\overline{V}} = \frac{\Delta A}{A} \tag{20}$$

It is reasonable to assume that the gain fluctuations and the random noise fluctuations are statistically independent. The net variance σ_v^2 of the output estimate is then determined for the total power radiometer from the expression

$$\left(\frac{\sigma_v}{\overline{V}}\right)^2 = \frac{2B_{no}}{B_{si}} + \left(\frac{\Delta A}{A}\right)^2 \tag{21}$$

The form of equation (21) is most convenient for statistically verifying the behavior of the radiometer simulations. However, the form most widely used in the literature employs the term "sensitivity." The sensitivity ΔT of a radiometer is defined as the change in the input temperature which produces a change $\Delta\overline{V}$ in the output estimate equal to the RMS value σ_v of the net fluctuations. For the total power radiometer, the sensitivity is determined from the expression

$$\left(\frac{\Delta T}{T_s}\right)^2 = \frac{2B_{no}}{B_{si}} + \left(\frac{\Delta A}{A}\right)^2 \tag{22}$$

where $T_s = T_A + T_R$ is the system temperature.

For the Dicke square-wave correlated radiometer, the expressions for the variance and sensitivity are somewhat more involved. Specifically, in the absence of gain fluctuations, the standard deviation σ_{vn} due to noise fluctuations only is determined from the expression

$$\frac{\sigma_{vn}}{\overline{V}} = 2\sqrt{\frac{2B_{no}}{B_{si}}}\ \frac{T_{eff}}{|T_A - T_B|} \tag{23}$$

where T_{eff} is defined as the effective system temperature and is given by

$$T_{eff} = \left[\frac{(T_A + T_R)^2 + (T_B + T_R)^2}{2}\right]^{\frac{1}{2}} \tag{24}$$

If gain fluctuations are present, the variance of the estimate is determined from the expression

$$\left(\frac{\sigma_v}{\overline{V}}\right)^2 = 4\left(\frac{2B_{no}}{B_{si}}\right) \frac{T_{eff}^2}{(T_A - T_B)^2} + \left(\frac{\Delta A}{A}\right)^2 \tag{25}$$

The sensitivity ΔT is determined from the relationship

$$\frac{(\Delta T)^2}{(T_A - T_B)^2} = 4\left(\frac{2B_{no}}{B_{si}}\right) \frac{T_{eff}^2}{(T_A - T_B)^2} + \left(\frac{\Delta A}{A}\right)^2 \tag{26}$$

This writer has not been able thus far to find a completely conclusive development of the variance and sensitivity functions for a closed-loop radiometer. Based on the best available information, it appears that the expressions for the open-loop Dicke radiometer as given by equations (25) and (26) may be adapted with modification to the closed-loop system. The primary changes are as follows: (1) The effective system temperature of equation (24) reduces to $T_{eff} = T_B + T_R$. This result occurs because a sufficient amount of noise is added to T_A so that the Dicke switch "sees" $T_B + T_R$ on both halves of a switching cycle. (2) The value of B_{no} is based on the closed-loop low-pass form of the transfer function of the system. (3) Effects of gain fluctuations may be eliminated from the appropriate expressions for steady-state computations.

Based on the preceding assumptions, the variance and sensitivity functions for the closed-loop feedback noise-injection radiometer have the forms

$$\frac{\sigma_v}{\bar{V}} = 2\sqrt{\frac{2B_{no}}{B_{si}}} \quad \frac{T_B + T_R}{|T_A - T_B|} \tag{27}$$

and

$$\Delta T = 2\sqrt{\frac{2B_{no}}{B_{si}}} \quad (T_B + T_R) \tag{28}$$

where B_{no} is determined from the low-pass parameters of the closed-loop feedback model. Various simulations obtained thus far have produced results reasonably close to the values predicted by equation (28), but not enough data have been obtained yet to obtain a meaningful statistical verification of the equations. These relationships will be investigated further as new developments are obtained from work currently underway.

STATISTICAL VERIFICATION OF MODELS

Numerous computer simulation runs were made during the development of the various programs in order to check their validity. It would be very unwieldy and quite unnecessary to attempt to present all or even most of the results that were obtained. Instead, certain representative results are presented and discussed in order to properly verify the general validity of the models.

Because more attention was paid to the basic total power radiometer early in the simulation development as a means of establishing proper direction, more of the data from those simulations were scrutinized from a statistical point of view. However, the same techniques have been applied in varying degrees to all of the simulation models. Close statistical comparison has been achieved for the Dicke open-loop radiometer models, and, as previously noted, trends obtained from the closed-loop models appear good and will be pursued further as accompanying analytical work is completed.

The various data selected for this report are summarized in tabular form in the Appendix. Each page contains a separate table, and a given table represents a particular set of simulation runs with fixed parameters. A list of all the table symbols is provided at the beginning of the Appendix and should be used for checking symbols in the tables.

A number of simulations was made using a running integrator. The output of a running integrator is a nonstationary process since the variance decreases with time. In order to provide a suitable means for determining the statistics at a given time, the concept of ensemble averaging was employed. This was achieved by using a number of separate simulation runs for fixed system parameters, but with each run utilizing statistically independent random generators. At a given value of time, true ensemble averaging could thus be achieved by performing appropriate averaging on the corresponding values from all of the separate runs. For most of the ensemble averages, either 6 or 11 runs were used. Actually, the ensemble averages were also used in some cases in which the output filters were not running integrators and in which the processes were stationary due to the convenience of the procedures already established.

The first representative simulation presented is that of a total power radiometer with TA = 100°, TR = 200°, BCIN = 1000 Hz (3-dB bandwidth and a 10-pole Butterworth filter), a running integrator at the output, no gain fluctuations, and a sampling rate of 10 KHz (DELT = 10^{-4} s). This simulation was performed in CSMP, and the results are summarized in table A-1. The terminology used at the bottom of the table refers to that employed in the actual program and is more convenient for listing than the usual subscript notation. For a 10-pole Butterworth filter, the equivalent noise bandwidth was calculated to be 1.004 times the 3-dB bandwidth, while the equivalent statistical bandwidth was calculated to be 1.057 times the 3-dB bandwidth. The former constant is so close to unity that it was ignored in the system constants for 10-pole calculations, but the latter constant was utilized. The predicted value of the standard deviation is determined from the relationship

$$\sigma_T = \frac{300}{\sqrt{1.057 \times 10^3 T}} \tag{29}$$

From table A-1, the predicted standard deviation σ_T values at different times and the measured estimates s_T are readily compared, and the results are seen to be quite good in a statistical sense. The confidence ranges for the mean and variance estimates were determined by standard statistical methods provided by Bendat and Piersol (ref. 5).

Table A-2 provides similar data obtained from a CSMP simulation when the input filter is eliminated. This means that the full sampled bandwidth (5 KHz in this case) is applied to the square-law detector. The predicted standard deviation in this case is

$$\sigma_T = \frac{300}{\sqrt{5000T}} \tag{30}$$

Table A-3 shows the results of a set of CSMP simulations having parameters similar to table A-1, but with gain fluctuations added. The reference level of the voltage gain is A = 1, and the fluctuations were introduced after the square-law detector. The predicted value of σ_T in this case is

$$\sigma_T = \sqrt{\frac{1}{1.057 \times 10^3 T} + (0.03162)^2} \times 300 \qquad (31)$$

Table A-4 shows the results of CSMP simulations using the parameters of Table A-2 but with gain fluctuations added. The predicted value of σ_T is

$$\sigma_T = \sqrt{\frac{1}{5000T} + (0.03162)^2} \times 300 \qquad (32)$$

After the programs were converted to ACSL and transferred to NASA/LaRC, several different changes were made in the simulation models. Most significant was th change from a 10-pole Butterworth input filter to a 3-pole Butterworth input filter. This change was made in order to reduce the settling time for proper correlation with the Dicke radiometer forms as was discussed earlier in this report. Another change made for some of the simulations was the use of a 3-pole Butterworth low-pass filter for the postdetection output filter. In this case, the variance of the output estimate does not decrease with time <u>after</u> the filter has completely settled. For a 3-pole Butterworth filter, the equivalent noise bandwidth is 1.047 times the 3-dB bandwidth, and the equivalent statistical bandwidth is 1.257 times the 3-dB bandwidth. The first constant was incorporated in the normalized form of Boltzmann's constant, i. . $K_n = 1/(1.047\ B_{in})$, so that the temperature remains directly reading.

The results of one set of total power radiometer runs using ACSL and the changes just noted are summarized in table A-5. In this case, the 3-dB output bandwidth is 1 Hz so the settling time is slightly greater than 1 s. In fact, the filter has not fully settled for the data in the first column, so those results are not too valid. The predicted value of the standard deviation σ_T for all cases after the filter has settled is

$$\sigma_T = \sqrt{\frac{2 \times 1.047}{1.257 \times 1000}} \times 300 \qquad (33)$$

The next several tables of results apply to Dicke square-wave correlated simulation runs. Table A-6 shows some results obtained from a series of six statistically independent simulations using CSMP and parameters indicated in the table, including the use of a three-pole output filter. The predicted value of the standard deviation is

$$\sigma_T = 2\sqrt{\frac{2 \times 1.047}{1.257 \times 10^4}} \times T_{eff} \tag{34}$$

where

$$T_{eff} = \sqrt{\frac{(100 + 200)^2 + (300 + 200)^2}{2}} = 412.31 \tag{35}$$

Table A-7 shows the results of several Dicke simulations using ACSL and a running integrator for the output filter. The predicted standard deviation in this case is

$$\sigma_T = 2\sqrt{\frac{1}{1.257 \times 10^4 T}}\ T_{eff} \tag{36}$$

The results of adding gain fluctuations to the Dicke radiometer are illustrated by the data shown in table A-8. In this case AVDEL = 0.025 and the predicted value of the standard deviation is

$$\sigma_T = \sqrt{4\left(\frac{1}{1.257 \times 10^4 T}\right) T_{eff}^2 + (0.025)^2\ (200)^2} \tag{37}$$

A case in which the gain fluctuations are so large that they almost overshadow the noise fluctuations is shown in table A-9. In this case AVDEL = 0.1, and the predicted value of the standard deviation is

$$\sigma_T = \sqrt{4\left(\frac{1}{1.257 \times 10^4 T}\right) T_{eff}^2 + (0.1)^2\ (200)^2} \tag{38}$$

SUMMARY AND CONCLUSIONS

Dynamic computer simulation models for various types of microwave radiometers have been developed to assist in the evolution of new radiometer measurement systems and in evaluating the performance of existing systems. Both CSMP and ACSL have been proved quite adaptable for this purpose provided that the bandwidth times integration time product is normalized to a lower value for simulation purposes. The programs are currently available for usage, and the design of one existing system has already been extensively investigated with one of the programs.

The validity of most of the programs has been investigated using statistical tests, and the results have been shown to have excellent correlation with theoretical predictions. Refinement, improvement, and further statistical verification will be continued as one phase of a new contract currently in progress.

APPENDIX

TABULATION OF REPRESENTATIVE SIMULATION DATA

Symbols used in the simulation programs vary slightly in some cases from those used in general and analytical developments in the report due to the basic differences in the forms. The following symbols may appear throughout the tables and in the section "Statistical Verification of Models."

TA	brightness or antenna temperature (T_A) to be measured
TR	effective receiver noise temperature (T_R) referred to radiometer input
TB	reference comparison temperature (T_B) of constant temperature enclosure
TD	effective noise temperature (T_D) of noise-injection source
TEXCNS	excess noise temperature of noise-injection source = TD - TB
BCIN	bandwidth of wide-band input filter (usually 3-dB bandwidth)
BCOUT	bandwidth of narrow-band output filter (equal to equivalent noise bandwidth for running integrator and closed-loop systems and equal to 3-dB bandwidth in other cases)
AVDEL	per unit voltage gain fluctuation referred to a point at the output of the square-law detector
T	time of integration
DELT	time increment between successive samples in the simulation = 1/sampling rate
KFVG	forward voltage gain
KFPG	forward power gain
FSWTCH	Dicke switching frequency
KDIRCP	directional coupler noise power injection constant
KINT	integrator constant

$\bar{T}$ estimate of mean value of temperature determined as a sample mean = $\frac{1}{N}\sum_{i=1}^{N} T_i$

s_T^2 estimate of the variance of the process obtained as a sample variance = $\frac{1}{N-1}\sum_{i=1}^{N} (T_i - \bar{T})^2$

s_T estimate of the standard deviation of the process obtained as a sample standard deviation = $\sqrt{s_T^2}$

σ predicted value of the standard deviation of the process

$s_{\bar{T}}^2$ estimated variance of the sampling mean = $\frac{s_T^2}{N}$

$s_{\bar{T}}$ estimated standard deviation of the sampling mean = $\sqrt{s_{\bar{T}}^2}$

μ_2 upper bound of the 90 percent confidence range for T

μ_1 lower bound of the 90 percent confidence range for T

σ_2 upper bound of the 90 percent confidence range for σ_T

σ_1 lower bound of the 90 percent confidence range for σ_T

Using results from Bendat and Piersol (ref. 5) the 90 percent confidence ranges for T and σ_T satisfy the following relationships:

$$\bar{T} - s_{\bar{T}}\, t_{n,\alpha/2} \leq T \leq \bar{T} + s_{\bar{T}}\, t_{n,\alpha/2}$$

$$\frac{ns_T^2}{\chi^2_{n,\alpha/2}} \leq \sigma_T^2 \leq \frac{ns_T^2}{\chi^2_{n,(1-\alpha/2)}}$$

where $n = N - 1$ and $\alpha = 0.05$. The parameters required in the above equations are tabulated below for N = 11 and 6, which represent the most common values used in the simulations.

	N = 11	N = 6
$t_{n,\alpha/2}$	1.812	2.015
$\chi^2_{n,\alpha/2}$	18.31	11.07
$\chi^2_{n,(1-\alpha/2)}$	3.94	1.15

Table A-1. Total power radiometer CSMP simulation set A. (Tabulated values of runs are temperature estimates of TA + TR in kelvin).

RUN	T = 0.2 s	T = 0.4 s	T = 0.6 s	T = 0.8 s	T = 1.0 s
1	273.77	280.83	284.04	287.81	289.94
2	295.71	298.24	290.45	289.33	291.69
3	301.37	306.68	318.08	317.60	317.25
4	315.26	298.32	296.17	308.31	306.59
5	310.72	316.74	325.86	322.95	318.74
6	280.59	278.88	299.51	303.20	302.12
7	330.12	293.10	292.81	293.57	293.50
8	307.63	307.22	310.64	306.71	308.44
9	292.25	295.72	289.70	293.56	300.36
10	327.99	297.56	293.97	296.38	298.85
11	253.20	273.19	285.28	291.03	291.74
$\overline{T}$	298.96	295.13	298.77	300.95	301.75
s_T^2	542.02	172.67	186.40	138.97	101.65
s_T	23.28	13.14	13.65	11.79	10.08
σ_T	20.63	14.59	11.91	10.32	9.23
$s_{\overline{T}}^2$	49.27	15.70	16.95	12.63	9.24
$s_{\overline{T}}$	7.02	3.96	4.12	3.55	3.04
μ_2	311.68	302.31	306.24	307.38	307.26
μ_1	286.24	287.95	291.30	294.52	296.24
σ_2	37.09	20.93	21.75	18.78	16.06
σ_1	17.21	9.71	10.09	8.71	7.45

(All quantities are expressed in their basic units.)

TA = 100, TR = 200, BCIN = 1000 (10 pole), BCOUT = 0.5/T, AVDEL = 0, DELT = 10^{-4}

Table A-2. Total power radiometer CSMP simulation set B. (Tabulated values of runs are temperature estimates of TA + TR in kelvin).

RUN	T = 0.2 s	T = 0.4 s	T = 0.6 s	T = 0.8 s	T = 1.0 s
1	283.58	289.16	293.95	292.69	293.44
2	306.65	307.42	304.41	303.01	306.51
3	304.26	303.87	304.88	304.39	303.22
4	291.93	294.46	293.78	296.20	297.10
5	291.32	294.56	303.69	301.19	303.47
6	293.03	286.41	296.41	298.72	298.85
7	293.82	296.16	300.31	302.21	299.23
8	294.94	296.15	298.23	298.25	298.51
9	295.43	305.81	304.32	305.01	307.22
10	301.51	298.93	300.17	304.61	302.27
11	303.49	300.45	298.57	299.46	302.70
$\overline{T}$	296.36	297.58	299.88	300.52	301.14
s_T^2	47.44	43.28	16.89	15.09	17.07
s_T	6.89	6.58	4.11	3.88	4.13
σ_T	9.49	6.71	5.48	4.74	4.24
$s_{\overline{T}}^2$	4.31	3.93	1.54	1.37	1.55
$s_{\overline{T}}$	2.08	1.98	1.24	1.17	1.25
μ_2	300.13	301.17	302.13	302.64	303.41
μ_1	292.59	293.99	297.63	298.40	298.88
σ_2	10.97	10.48	6.55	6.19	6.58
σ_1	5.09	4.86	3.04	2.87	1.05

(All quantities are expressed in their basic units.)

TA = 100, TR = 200, BCIN = 5000 (no filter), BCOUT = 0.5/T, AVDEL = 0, DELT = 10^{-4}

Table A-3. Total power radiometer CSMP simulation set C. (Tabulated values of runs are temperature estimates of TA + TR in kelvin.)

RUN	T = 0.2 s	T = 0.4 s	T = 0.6 s	T = 0.8 s	T = 1.0 s
1	273.60	280.66	283.86	287.63	289.76
2	306.88	309.51	301.42	300.26	302.70
3	295.74	300.95	312.13	311.66	311.32
4	311.51	294.76	292.64	304.64	302.94
5	309.12	315.11	324.18	321.29	317.10
6	281.04	279.33	300.00	303.70	302.62
7	329.03	292.13	291.84	292.60	292.53
8	293.07	292.67	295.93	292.19	293.83
9	302.50	306.10	299.87	303.86	310.90
10	314.68	285.48	282.04	284.35	286.73
11	263.80	284.63	297.22	303.21	303.96
$\overline{T}$	298.27	294.67	298.28	300.49	301.31
s_T^2	372.76	143.54	142.96	116.08	93.38
s_T	19.31	11.98	11.96	10.77	9.66
σ_T	22.71	17.40	15.23	14.01	13.23
$s_{\overline{T}}^2$	33.89	13.05	13	10.55	8.49
$s_{\overline{T}}$	5.82	3.61	3.61	3.25	2.91
μ_2	308.82	301.21	304.82	306.38	306.58
μ_1	287.72	288.13	291.74	294.60	296.04
σ_2	30.76	19.09	19.05	17.16	15.39
σ_1	14.27	8.85	8.84	7.96	7.14

(All quantities are expressed in their basic units.)

TA = 100, TR = 200, BCIN = 1000 (10 pole), BCOUT = 0.5/T, AVDEL = 0.03162, DELT = 10^{-4}

Table A-4. Total power radiometer CSMP simulation set D. (Tabulated values of runs are temperature estimates of TA + TR in kelvin.)

RUN	T = 0.2 s	T = 0.4 s	T = 0.6 s	T = 0.8 s	T = 1.0 s
1	283.40	288.98	293.77	292.50	293.26
2	318.24	319.03	315.91	314.45	318.09
3	298.57	298.19	299.18	298.70	297.55
4	288.45	290.94	290.28	292.67	293.56
5	289.82	293.05	302.13	299.64	301.91
6	293.51	286.88	296.89	299.21	299.34
7	292.84	295.18	299.32	301.21	298.24
8	280.97	282.13	284.10	284.13	284.37
9	305.79	316.54	315.00	315.72	318.00
10	289.27	286.80	287.99	292.25	290.00
11	316.19	313.03	311.07	312.00	315.37
$\overline{T}$	296.10	297.34	299.60	300.23	300.88
s_T^2	154.59	167.18	114.46	102.52	132.33
s_T	12.43	12.93	10.70	10.13	11.50
σ_T	13.42	11.62	10.95	10.61	10.39
$s_{\overline{T}}^2$	14.05	15.20	10.41	9.32	12.03
$s_{\overline{T}}$	3.75	3.90	3.23	3.05	3.47
μ_2	302.90	304.41	305.45	305.76	307.17
μ_1	289.31	290.27	293.75	294.70	294.59
σ_2	19.81	20.60	17.04	16.13	18.33
σ_1	9.19	9.56	7.91	7.48	8.50

(All quantities are expressed in their basic units.)

TA = 100, TR = 200, BCIN = 5000 (no filter), BCOUT = 0.5/T, ΔA = 0.03162, DELT = 10^{-4}

Table A-5. Total power radiometer ACSL simulation set A. (Tabulated values of runs are temperature estimates of TA + TR in kelvin.)

RUN	T = 1.0 s	T = 1.5 s	T = 2.0 s	T = 2.5 s	T = 3.0 s	T = 3.5 s	T = 4.0 s	T = 4.5 s	T = 5.0 s
1	346.87	295.45	277.01	281.29	282.76	282.40	286.47	311.82	313.3
2	302.32	305.75	312.50	292.86	303.09	298.65	295.99	295.15	276.99
3	307.08	311.12	307.27	311.42	292.91	280.58	292.81	308.02	295.28
4	317.28	303.00	288.10	279.31	284.97	293.71	297.18	294.20	276.12
5	296.78	289.26	300.55	300.21	282.85	300.73	302.70	286.20	297.32
6	287.54	289.66	308.55	296.83	288.80	285.24	300.78	287.45	323.14
7	290.22	294.27	298.68	304.32	300.16	307.19	287.08	304.41	293.67
8	322.53	301.46	283.81	308.69	303.16	305.62	305.55	297.32	295.28
9	304.20	285.28	288.42	289.96	286.31	295.86	305.34	271.99	284.01
10	312.32	307.02	297.34	302.25	309.09	296.22	316.80	298.20	326.72
11	304.72	287.37	295.19	276.26	302.80	289.86	296.71	308.18	299.03
$\overline{T}$	308.35	297.72	296.13	294.85	294.26	294.19	298.86	296.63	298.26
s_T^2	274.49	78.53	121.60	144.20	92.86	79.25	77.16	136.56	284.11
s_T	16.57	8.86	11.03	12.01	9.64	8.90	8.78	11.69	16.86
σ_T	12.24	12.24	12.24	12.24	12.24	12.24	12.24	12.24	12.24
$s_{\overline{T}}^2$	24.95	7.14	11.05	13.11	8.44	7.20	7.01	12.41	25.83
$s_{\overline{T}}$	5.00	2.67	3.32	3.62	2.91	2.68	2.65	3.52	5.08
μ_2	317.41	302.56	302.15	301.41	299.53	299.05	303.66	303.01	307.46
μ_1	299.29	292.88	290.11	288.29	288.99	289.33	294.06	290.25	289.06
σ_2	26.39	14.12	17.57	19.13	15.35	14.18	13.99	18.62	26.85
σ_1	12.24	6.55	8.15	8.87	7.12	6.58	6.49	8.64	12.46

(All quantities are expressed in their basic units.)

TA = 100, TR = 200, BCIN = 1000 (3 pole), BCOUT = 1(3 pole), ΔA = 0, DELT = 10^{-4}

Table A-6. Dicke square-wave correlated CSMP simulation set A. (Tabulated values of runs are temperature estimates of TB - TA in Kelvin.)

RUN	T = 1.0 s	T = 1.2 s	T = 1.4 s	T = 1.6 s	T = 1.8 s	T = 2.0 s
1	204.12	202.00	209.02	202.81	189.04	180.60
2	205.67	199.29	206.45	206.57	211.49	204.34
3	191.48	185.35	181.01	181.39	182.73	191.20
4	179.19	177.01	190.97	205.88	209.80	202.48
5	209.93	209.86	201.81	180.74	176.24	176.11
6	188.40	192.96	201.28	208.43	212.33	199.98
$\overline{T}$	196.47	194.41	198.42	197.64	196.94	192.45
s_T^2	142.59	141.41	111.02	168.09	261.35	141.53
s_T	11.94	11.89	10.54	12.97	16.17	11.90
σ_T	10.64	10.64	10.64	10.64	10.64	10.64
$s_{\overline{T}}^2$	23.77	23.57	18.50	28.02	43.56	23.59
$s_{\overline{T}}$	4.87	4.85	4.30	5.29	6.60	4.86
μ_2	206.28	204.18	207.08	208.30	210.24	202.24
μ_1	186.66	184.64	189.76	186.98	183.64	182.66
σ_2	24.90	24.80	21.97	27.03	33.71	24.81
σ_1	8.03	7.99	7.08	8.71	10.86	8.00

(All quantities are expressed in their basic units.)

TA = 100, TB = 300, TR = 200, BCIN = 10^4 (3 pole), BCOUT = 1 (3 pole), ΔA = 0, DELT = 10^{-5}, FSWTCH = 100

Table A-7. Dicke square-wave correlated ACSL simulation set A. (Tabulated values of runs are temperature estimates of TB - TA in Kelvin.)

RUN	T = 0.5 s	T = 1.0 s	T = 1.5 s	T = 2.0 s	T = 2.5 s	T = 3.0 s	T = 3.5 s	T = 4.0 s	T = 4.5 s	T = 5.0 s
1	186.14	200.72	196.72	195.88	194.92	194.50	193.14	194.03	193.01	192.33
2	202.49	196.22	199.54	199.58	195.43	197.36	197.43	196.82	195.92	195.69
3	187.89	196.40	193.26	195.83	190.82	191.13	192.82	191.98	190.22	193.09
4	208.48	206.62	207.68	205.29	205.28	202.62	199.57	198.06	199.22	199.78
5	184.60	185.58	189.94	193.30	194.07	190.94	189.46	189.11	190.01	190.02
6	190.72	192.06	196.28	198.77	196.60	197.92	197.11	197.14	196.84	197.12
$\bar{T}$	193.39	196.27	197.24	198.11	196.19	195.75	194.92	194.52	194.20	194.67
s_T^2	95.54	51.79	36.92	17.49	23.66	20.11	14.02	12.13	13.99	12.55
s_T	9.77	7.20	6.08	4.18	4.86	4.48	3.74	3.48	3.74	3.54
σ_T	10.40	7.36	6.01	5.20	4.65	4.2[illegible]	3.93	3.68	3.47	3.29
$s_{\bar{T}}^2$	15.92	8.63	6.15	2.92	3.94	3.35	2.34	2.02	2.33	2.09
$s_{\bar{T}}$	3.99	2.94	2.48	1.71	1.99	1.83	1.53	1.42	1.53	1.45
μ_2	201.43	202.19	202.24	201.56	200.20	199.44	198.00	197.38	197.28	197.59
μ_1	185.35	190.35	192.24	194.66	192.18	192.06	191.84	191.66	191.12	192.66
σ_2	20.38	15.01	12.67	8.72	10.14	9.35	7.81	7.26	7.80	7.39
σ_1	6.57	4.84	4.08	2.81	3.27	3.01	2.52	2.34	2.51	2.38

(All quantities are expressed in their basic units.)

TA = 100, TB = 300, TR = 200, BCIN = 10^4 (3 pole), BCOUT = $0.5/\tau$, ΔA = 0, DELT = 10^{-5}, FSWTCH = 100

Table A-8. Dicke square-wave correlated ACSL simulation set B. (Tabulated values of runs are temperature estimates of TB - TA in kelvin.)

RUN	T = 0.5 s	T = 1.0 s	T = 1.5 s	T = 2.0 s	T = 2.5 s	T = 3.0 s	T = 3.5 s	T = 4.0 s	T = 4.5 s	T = 5.0 s
1	186.18	200.77	196.77	195.93	194.96	194.79	193.18	194.08	193.06	192.37
2	209.34	202.86	206.29	206.32	202.04	204.04	204.11	203.48	202.54	202.31
3	193.43	191.45	195.66	198.14	195.98	197.10	196.49	196.51	196.21	196.50
4	213.14	211.23	212.33	209.88	209.86	207.15	204.03	202.49	203.68	204.24
5	172.08	177.15	181.32	184.52	185.26	182.27	180.86	180.53	181.39	181.39
6	185.87	194.30	191.18	193.72	188.77	189.08	190.75	189.92	188.18	191.02
$\bar{T}$	193.34	196.29	197.26	198.09	196.15	195.74	194.90	194.50	194.18	194.64
s_T^2	241.42	136.03	120.50	82.93	79.43	85.53	77.60	72.86	73.02	69.65
s_T	15.54	11.66	10.98	9.11	8.91	9.25	8.81	8.54	8.55	8.35
σ_T	11.54	8.89	7.82	7.22	6.83	6.56	6.36	6.21	6.08	5.99
$s_{\bar{T}}^2$	40.24	22.67	20.08	13.82	13.24	14.25	12.93	12.14	12.17	11.61
$s_{\bar{T}}$	6.34	4.76	4.48	3.72	3.64	3.78	3.60	3.48	3.49	3.41
μ_2	206.12	205.88	206.29	205.59	203.48	203.36	202.15	201.51	201.21	201.51
μ_1	180.56	186.70	188.23	190.59	188.82	188.12	187.65	187.49	187.15	187.77
σ_2	32.40	24.32	22.89	18.99	18.58	19.28	18.37	17.80	17.82	17.40
σ_1	10.44	7.84	7.38	6.12	5.99	6.22	5.92	5.74	5.74	5.61

(All quantities are expressed in their basic units.)

TA = 100, TB = 300, TR = 200, BCIN = 10^4 (3 pole), BCOUT = 0.5/T, AVDEL = 0.025, DELT = 10^{-5}, FSWTCH = 100.

Table A-9. Dicke square-wave correlated ACSL simulation set C. (Tabulated values of runs are temperature estimates of TB - TA in kelvin.)

RUN	T = 0.5 s	T = 1.0 s	T = 1.5 s	T = 2.0 s	T = 2.5 s	T = 3.0 s	T = 3.5 s	T = 4.0 s	T = 4.5 s	T = 5.0 s
1	186.30	200.89	196.89	196.05	195.09	194.91	193.31	194.20	193.18	192.49
2	229.89	222.77	226.54	226.57	221.87	224.06	224.14	223.45	222.42	222.17
3	191.58	189.62	193.20	196.24	194.10	195.40	194.60	194.63	194.33	194.61
4	227.12	225.19	226.25	223.65	223.62	220.73	217.41	215.77	217.04	217.64
5	147.53	151.88	155.45	158.20	158.82	156.26	155.06	154.77	155.51	155.51
6	179.82	187.97	184.96	187.42	182.62	182.92	184.54	183.73	182.06	184.80
$\bar{T}$	193.71	196.39	197.22	198.02	196.02	195.71	194.84	194.42	194.09	194.54
s_T^2	962.04	728.69	722.74	635.41	599.59	630.07	611.77	597.01	592.66	583.89
s_T	31.02	26.99	26.88	25.21	24.49	25.10	24.73	24.43	24.43	24.16
σ_T	22.54	21.31	20.88	20.66	20.53	20.45	20.38	20.34	20.30	20.27
$s_{\bar{T}}^2$	160.34	121.45	120.46	105.90	99.93	105.01	101.96	99.50	98.78	97.31
$s_{\bar{T}}$	12.66	11.02	10.98	10.29	10.00	10.25	10.10	9.98	9.94	9.86
μ_2	219.22	218.60	219.34	218.75	216.17	216.36	215.19	214.53	214.12	214.41
μ_1	168.20	174.18	175.10	177.29	175.87	175 06	174.49	174.31	174.06	174.67
σ_2	64.67	56.29	56.06	52.56	51.06	52.34	51.57	50.95	50.76	50.38
σ_1	20.85	18.14	18.07	16.94	16.46	16.37	16.62	16.42	16.36	16.24

(All quantities are expressed in their basic units.)

TA = 100, TB = 300, TR = 200, BCIN = 10^4 (3 pole), BCOUT = 0.5/Γ, AVDEL = 0.1, DELT = 10^{-5}, FSWTCH = 100.

REFERENCES

1. System/360 Continuous System Modeling Program (360A-CS-16X) Application Description. 4th Ed. IBM GH20-0240-3, Mar. 1972.

2. System/360 Continuous System Modeling Program Users Manual, Program #360A-CX-16X. 4th Ed. IBM GH20-0567-4, Jan. 1972.

3. Speckhart, F.H.; and Green, W.L.: A Guide to Using CSMP. Prentice Hall, Inc. (Englewood Cliffs, NJ), 1976.

4. Mitchell & Gauthier Associates: Advanced Continuous Simulation Language (ACSL) User Guide/Reference Manual.

5. Bendat, J.S.; and Piersol, A.G.: Random Data: Analysis and Measurement Procedures, John Wiley and Sons, Inc. (NY), 1971.

6. Tiuri, M.E.: Radio Astronomy Receivers. IEEE Trans. Antennas Prop., Vol. AP-12, Dec. 1964, pp. 930-938.

7. Evans, G.; and McLeish, C.W.: RF Radiometer Handbook. Artech House (Dedham, MA), 1977.

8. Dicke, R.H.: The Measurement of Thermal Radiation at Microwave Frequencies. Rev. Sci. Instr., Vol. 17, July 1946, pp. 268-275.

9. Hardy, W.N.; Gray, K.W.; and Love, A.W.: An S-Band Radiometer Design with High Absolute Precision. IEEE Trans. Microwave Theory & Technique, Vol. MTT-22, Apr. 1974, pp. 382-390.

ADDITIONAL PUBLICATIONS RESULTING FROM RESEARCH

The two following additional publications have resulted from this contract. Full acknowledgment of support from NASA was given in both cases.

Stanley, W.D.; Harrington, R.F.; and Lawrence, R.W.: Dynamic Simulation of Random Processes in Radiometers Using CSMP and ACSL. Presented at IEEE SOUTHEASCON Conference, Roanoke, VA, Apr. 1979; also published in SOUTHEASCON 1979 Conference Proceedings.

Stanley, W.D.; and Peterson, S.J.: Equivalent Statistical Bandwidths of Conventional Low-Pass Filters. To be published in IEEE Trans. Communications.

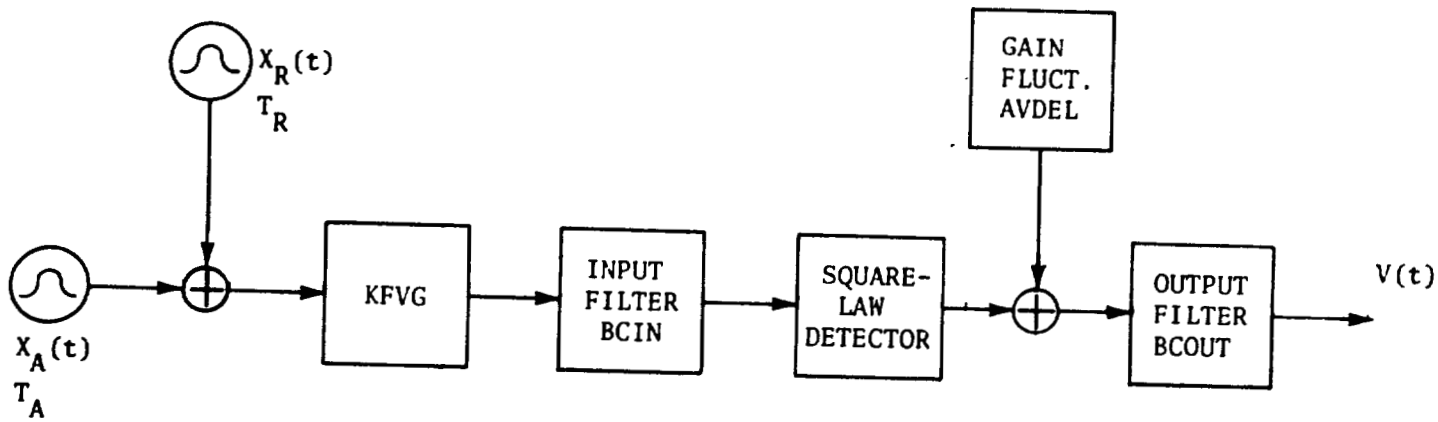

Figure 1. Block diagram of total power simulation models.

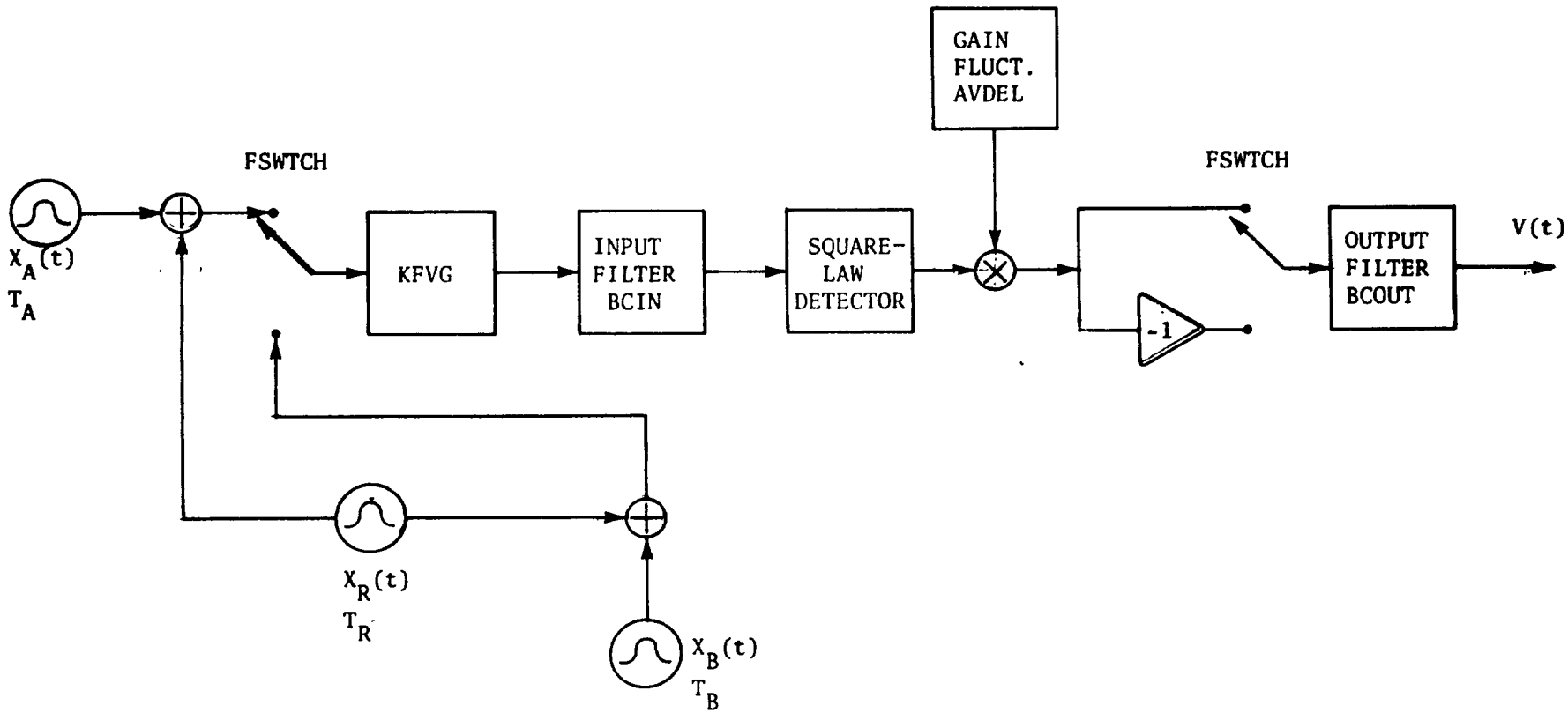

Figure 2. Block diagram of open-loop Dicke square-wave correlated simulation models.

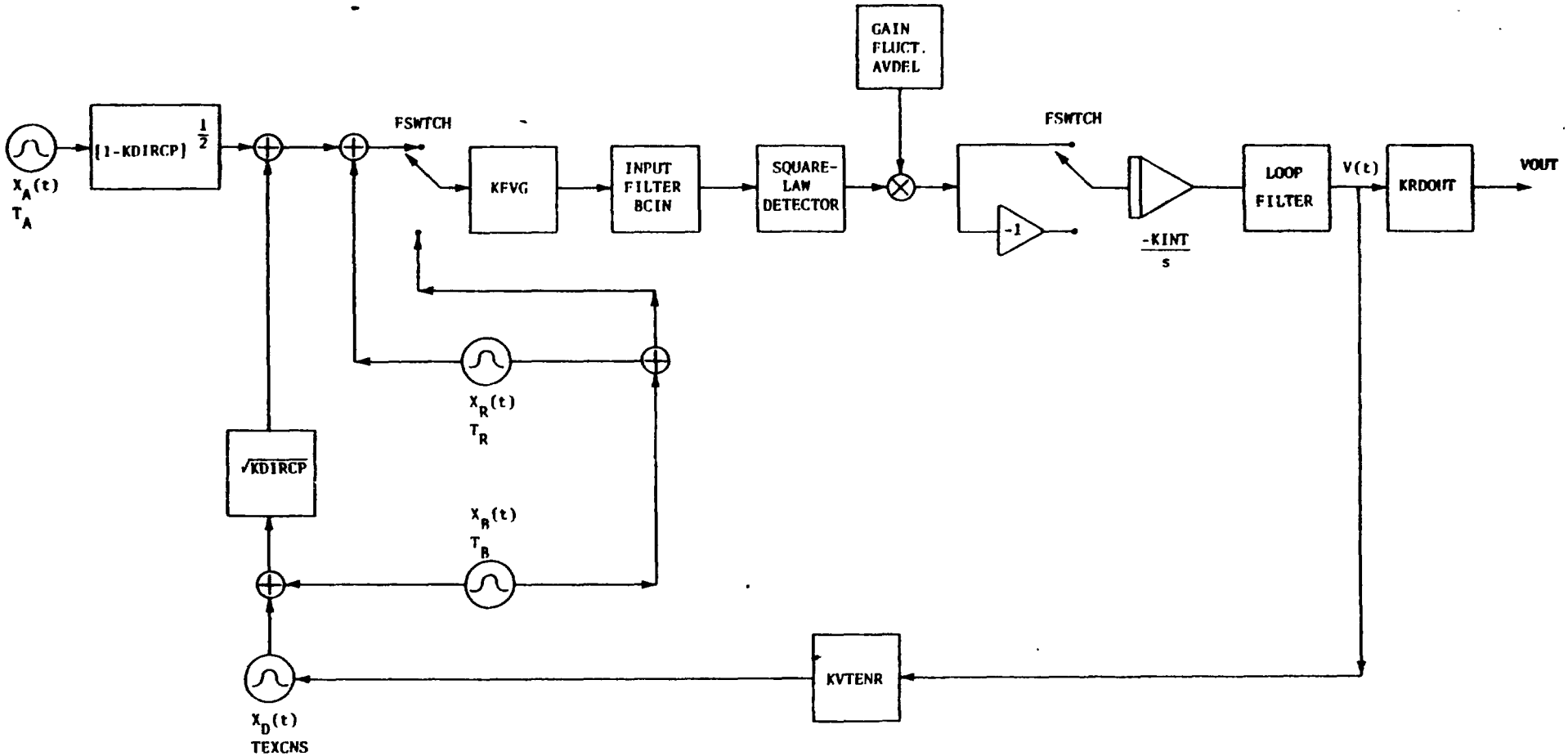

Figure 3. Block diagram of closed-loop, noise-injection, feedback statistical radiometer models.

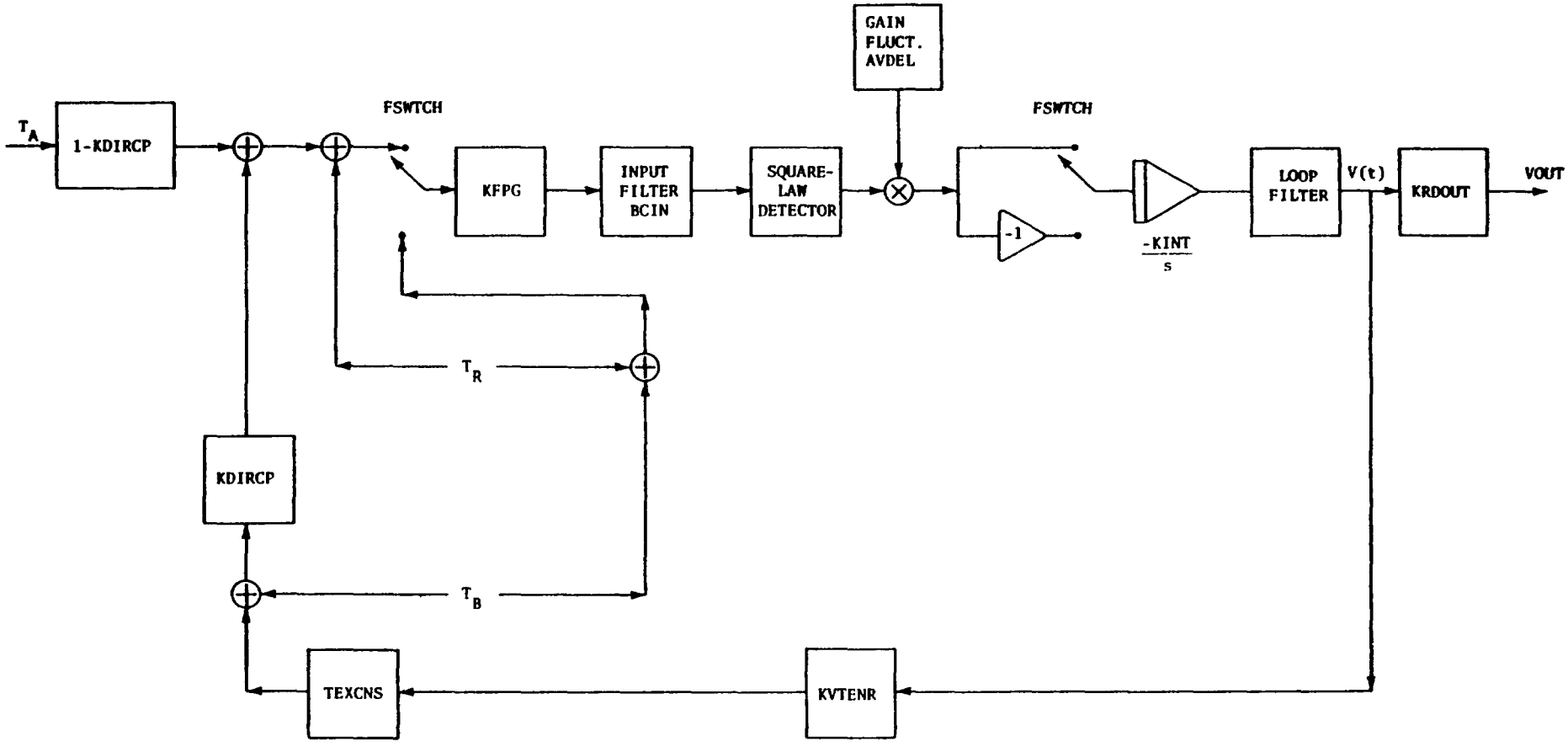

Figure 4. Block diagram of closed-loop, noise injection, feedback deterministic radiometer models.